International Journal of Electrical, Electronic and Communication Sciences
ISSN: 2517-9438
Vol:2, No:10, 2008

Optimal Control Strategy for High Performance EV Interior Permanent Magnet Synchronous Motor

Mehdi Karbalaye Zadeh, and Ehsan M. Siavashi

***Abstract*—**The controllable electrical loss which consists of the copper loss and iron loss can be minimized by the optimal control of the armature current vector. The control algorithm of current vector minimizing the electrical loss is proposed and the optimal current vector can be decided according to the operating speed and the load conditions. The proposed control algorithm is applied to the experimental PM motor drive system and this paper presents a modern approach of speed control for permanent magnet synchronous motor (PMSM) applied for Electric Vehicle using a nonlinear control. The regulation algorithms are based on the feedback linearization technique. The direct component of the current is controlled to be zero which insures the maximum torque operation.

The near unity power factor operation is also achieved. More over, among EV's motor electric propulsion features, the energy efficiency is a basic characteristic that is influenced by vehicle dynamics and system architecture. For this reason, the EV dynamics are taken into account.

***Keywords*—**PMSM, Electric Vehicle, Optimal control, Traction.

I. Introduction

THE main capabilities required in the applications such as traction motor for a hybrid electric vehicle and ISG (Integrated Starter Generator) are wide constant power speed range (CPSR) and high efficiency. Interior PM synchronous motor (IPMSM) is one of the motors suitable for the applications [1]. From the torque performance point of view, however, the IPMSM has two drawbacks. That is, torque ripple and cogging torque are relatively large as compared with a surface PM synchronous motor. Moreover, the IPMSM with concentrated winding is more disadvantageous than that with distributed winding in the respects [2].

These problems are produced mostly by the discontinuous reluctance variation because of the slotted structure of stator core and saturation of magnetic circuit [2], [3]. Particularly, the magnetic saturation of the IPMSM operated in wide speed range through flux weakening control greatly varies according to load condition.

M. Karbalaey Zadeh is with the Electrical Engineering Department, Engineering Facalty, University of Tehran, Tehran, Iran (e-mail: bardia2551@ yahoo.com).

E. M. Siavashi is with the Electrical Engineering Department, Engineering Facalty, University of Tehran, Tehran, Iran (e-mail: esiavashi@ ut.ac.ir).

TABLE I
Specifications of Initial Designed IPMSM

Items	Values
Stator outer diameter	292 mm
Rotor outer diameter	204.8 mm
Stack length	85 mm
Air-gap	0.9 mm
Br (@120oC)	1.103 T
Number of poles	12
DC link voltage	320 V
Rated output power	20 kW
Rated current	70 A rms
Base and maximum speed	680, 3400

Thus, the optimal design of IPMSM is demanded in order to improve torque performance.

In this paper, each optimal model minimizing torque ripple at the base and maximum speed and cogging torque is investigated by an optimization method without a great change of the motor parameters in the initial designed IPMSM. In addition, the characteristics of each model are compared by Finite Element Analysis (FEA) and characteristic equation. In the end, the final results show the optimal shape according to the operating point of IPMSM must be changed to enhance torque characteristic.

II. PM Model and Equivalent Circuit

Fig. 1 displays the configuration of the initial designed IPMSM with concentrated winding. The CPSR of the initial model is from 680 rpm to 3400 rpm, and the main dimension and specifications are listed in Table I.

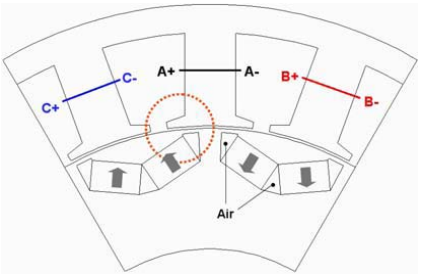

Fig. 1 Configuration of initial designed IPMSM

Equivalent circuits for the characteristic analysis of the IPMSM are shown in Fig. 2 [4]. The equivalent circuits include the effects of the copper loss and the iron loss.

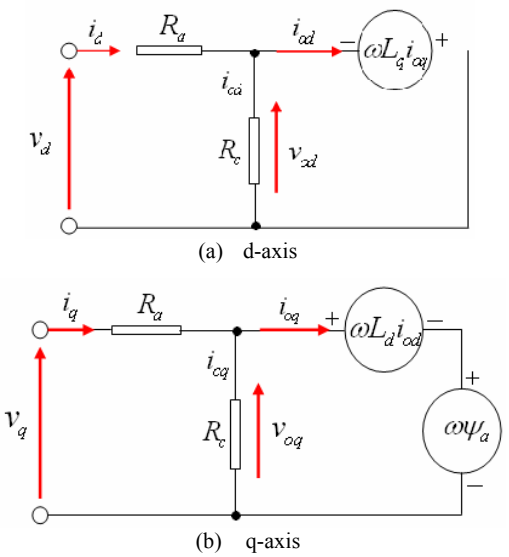

Fig. 2 Equivalent circuits of IPMSM

From Fig. 2, the voltage and effective torque equation of the IPMSM in the steady-state are expressed as follows:

$$V_d = r_s + \mathrm{P}\lambda_d - w_e\lambda_q \quad (1)$$

$$V_q = r_s + \mathrm{P}\lambda_q + w_e\lambda_d \quad (2)$$

$$\lambda_q = (L_{ls} + L_{mq})I_q \quad (3)$$

$$\lambda_d = (L_{ls} + L_{md})I_d + \lambda_m \quad (4)$$

$$T = Pn[\psi_\alpha i_{oq} + (L_d - L_q)i_{od}i_{oq}] \quad (5)$$

Where i_d, i_q : d and q-axis components of armature current; i_{od} , i_{oq} : d and q- axis component of iron loss current ; v_d, v_q: d,q component of terminal voltage ; ψ_a ; $(\sqrt{3}/2)\psi_f$; ψ_f: Maximum flux linkage of permanent magnet; R_a : armature winding resistance; R_c: iron loss resistance; L_d, L_q: inductance along d-axis and q-axis; P_n: number of pole pairs.

III. Parameter Calculation Method and Initial Conditions for Optimization

There are four parameters, ψ_a, R_a, R_c, L_d and L_q, needed to solve the circuit models of Fig. 2. In this paper, the estimation method on two parameters of them, iron loss resistance and inductances, is introduced, and then the characteristics of the initial model obtained by the circuits based on the parameters are finally displayed in Section V.

A. Equivalent Iron Loss Resistance, R_c

Fig. 3 shows the procedure of iron loss calculation using iron loss data of magnetic material.

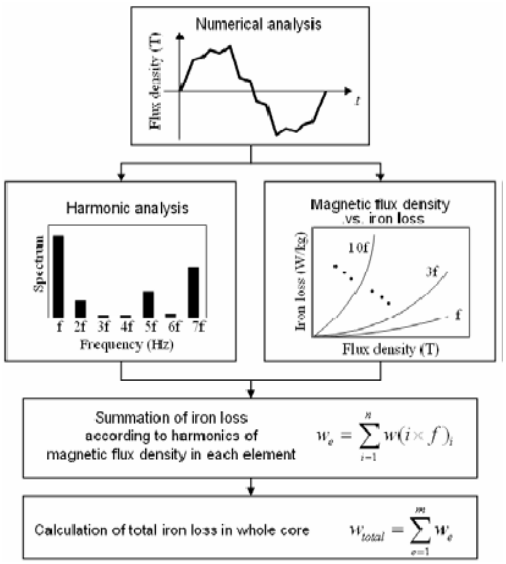

Fig. 3 Calculation process of iron loss.

The detail explanation as regards the flowchart has been given in [5]. After calculating total iron loss, w_{total}, the iron loss resistance R_c is calculated by(6).

$$\mathrm{R_c} = \frac{\mathrm{v_{o2}}}{\mathrm{w_{total}}} \quad (6)$$

where v_0 is terminal voltage at the no load and 1000 rpm.

B. Inductances, Ld and L_q

At the base and maximum speed, input armature current and current angle (β) are demanded to estimate accurately torque ripple by FEA. To get them, L_d and L_q must be computed according to the variation of armature current and β. In this paper, they are obtained by FEA, cubic spline interpolation and (5). In (5), ψ_a and ψ_o are fundamental components calculated from fourier analysis. The steady-state phasor diagram of IPMSM is shown in Fig. 4 [6].

$$\mathrm{L_d} = \frac{(\psi_o \cos\alpha - \psi_a)}{\mathrm{i_d}} \quad , \quad \mathrm{L_q} = \frac{\psi_o \sin\alpha}{\mathrm{i_q}} \quad (7)$$

where ψ_o: total flux linkage considering the armature reaction effects; α: phase difference between ψ_a and ψ_o.

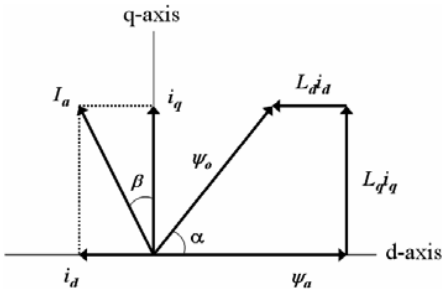

Fig. 4 Phasor diagram of IPMSM

C. Results of Initial Model by Characteristic Equation

The characteristics of the initial model are predicted with L_d and L_q estimated through the way mentioned above. At this time, the limitations on armature current and terminal voltage are considered as (8) and (9), and in this stage, all the losses except the copper loss are ignored.

$$I_a = \sqrt{i_d^2 + i_q^2} \le I_{am} \quad (8)$$

$$V_a = \sqrt{v_d^2 + v_q^2} \le V_{am} \quad (9)$$

where I_{am}, V_{am}: peak values of current and voltage.

The entire torque-speed operation region considering the above control conditions is acquired as the following manner. In the anterior region of base speed, maximum torque per ampere control is used, and flux weakening control is applied in the posterior region. In the end, the characteristics obtained from the initial model satisfy the specifications given in Table I, and torque ripple at the base and maximum speed and peak value of cogging torque are 22 %, 184 % and 4.03 Nm respectively. At that time, input current is 64.2 A and 63.1 A, and β is 39.2o and 80.6o, and the optimization process of the IPMSM is based on these results.

IV. Optimization

A. Design Variables for Optimization

In the IPMSM, the operating limits, restrictions on current and terminal voltage, and CPSR critically depend on the motor parameters such as flux linkage generated by permanent magnet and inductance [7]. Therefore, in the initial model, the size and position of permanent magnet and air-gap length are not changed, because they greatly affect the parameters. Due to fill factor, the teeth and yoke width are not altered as well. Thus, design variables selected in this paper are barrier angle (BA), chamfer (C), slot opening (SO). Fig. 5, the magnified figure of the part surrounded a dotted line in Fig. 1, shows them.

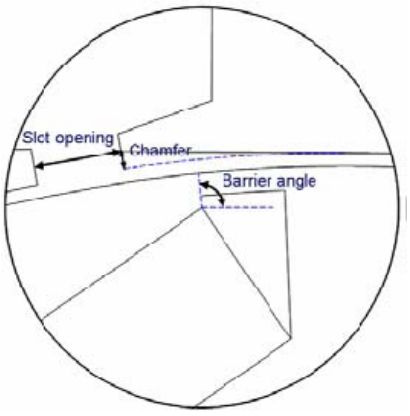

Fig. 5 Design variables for optimization

B. Experimental Design

In this paper, full factorial design (FFD), one of the experimental designs, is used, and the reason is written as follows. First, all combinations of the design variables chosen in the initial model are inspected, and interaction effects between them are evaluated without confounding. Moreover, the main factors on torque ripple and cogging torque are detected by analysis-of-variance (ANOVA). Second, the prediction of the responses according to the variation of the design factors is possible. Finally, the effective and reasonable design area is selected to apply response surface method (RSM) [8], [9]. In the motor design, to research the full design region needs a lot of modeling and computing time. In addition, in RSM, the accuracy of approximation greatly depends on the size of the space in which the design parameters may vary [10]. Accordingly, FFD is performed in the wide domain, and then RSM is applied in the best region searched by that.

Table II shows the array of 2^3 FFD to examine torque ripple and cogging torque. In the table, experiment No. 9 is added to estimate the curvature in the middle point of each design area, because it is performed at only two levels. In this paper, the levels are called "low" and "high" and denoted as "−1" and "+1" respectively.

In this paper, ANOVA is applied to evaluate more objectively the significance of each design factor through statistical analysis. At that time, there is no replication of experiment. ANOVA table is shown in Table III. In the table, the sums of squares (*SS*) of each term and those of error and total term are given as follows:

$$SS_{Term} = \frac{1}{N[total\ sum\ of\ high\ levels - total\ sum\ of\ low\ levels]} \quad (10)$$

$$SS_E = SS_T - [SS_{BA} + SS_C + SS_{SO} + SS_{BA*C} + SS_{BA*SO} + SS_{C*SO}] \quad (11)$$

$$SS_T = \sum_{i=1}^{l\times m\times n} y_i^2 - \frac{(\sum_{i=1}^{l\times m\times n} y_i)^2}{l\times m\times n} \quad (12)$$

Where N: total number of trials; y_i: *i-th* response value in the experiment; l, m and n: the number of levels in factor BA, C and SO respectively. The ANOVA results of each response are listed in Table IV, Table V and Table VI. Especially, in the tables, the important factors on the each response are indicated at 5% and 10% significance level [8]. Fig. 6 shows the variation of each response according to main factors based on ANOVA results. In Fig. 6. (c), the interaction effect plot between BA and C is displayed, and the peak-to-peak value of cogging torque is small overall when BA is 34.5°. However, in the value of BA, the aspects of torque ripple at the maximum speed and cogging torque according to C occur by contraries. Therefore, in the optimal stage applied with RSM, the scope of C is the same that used in FFD.

TABLE II
ARRAY OF 2^3 FFD AND RESULTS

Experiment No.	BA[°] (level)	C[mm] (level)	SO[mm] (level)	BA*C (leve)	BA*SO (level)	C*SO (level)
1	34.5(-1)	0.5(-1)	4(-1)	(+1)	(+1)	(+1)
2	145.5(+1)	0.5(-1)	4(-1)	(-1)	(-1)	(+1)
3	34.5(-1)	1.5(+1)	4(-1)	(-1)	(+1)	(-1)
4	145.5(+1)	1.5(+1)	4(-1)	(+1)	(-1)	(-1)
5	34.5(-1)	0.5(-1)	8(+1)	(+1)	(-1)	(-1)
6	145.5(+1)	0.5(-1)	8(+1)	(-1)	(+1)	(-1)
7	34.5(-1)	1.5(+1)	8(+1)	(-1)	(-1)	(+1)

Ex .No	Torque . ripple[%] @ base speed	Torque. ripple[%] @ max. speed	Cogging T_{p-p} [Nm]
1	22.2	108.2	0.88
2	22.8	109.4	8.76
3	17.6	46.0	4.44
4	17.2	49.0	4.63
5	8.6	79.8	1.19
6	10.3	91.3	6.86
8	11.2	38.6	6.56
9	14.8	90.2	1.61

C. RSM

RSM is a set of statistical and mathematical techniques to find the "best fitted" response of the physical system through experiment or simulation. It has recently been recognized as an effective approach for modeling the performance of electrical devices. In RSM, a polynomial model called a fitted model is generally to be constructed to represent the relationship between the performance and design parameters [9]. Thus, this model provides designers with an overall prospect of the performance according to the behavior of the factors in a design space. In this paper, RSM is employed to make appropriate response models with respect to torque ripple and cogging torque in the initial designed IPMSM. In general, the response model can be written as follows:

$$Y = \beta_0 + \sum_{i=1}^{k} \beta_i x_i + \sum_{i=1}^{k} \beta_{ii} x_i^2 + \sum_{i=1}^{k} \beta_{ij} x_i x_j + \xi \qquad (13)$$

Where β is regression coefficients for design variables, ξ is random error treated statistical error.

In this paper, least square method is utilized to estimate unknown coefficients, and the fitted coefficients and the fitted response model can be written as:

$$\beta\hat{} = (X'Y)^{-1} X'Y \qquad (14)$$

Where X: matrix notation of the levels of the independent variables; X': transpose of the matrix X; Y: vector of the observations.

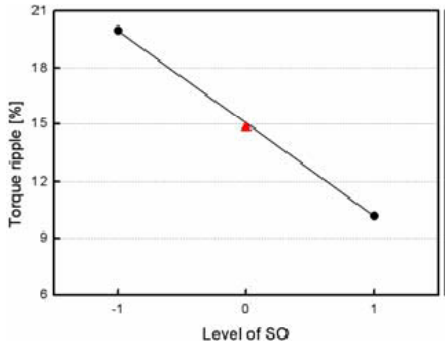

(a) Torque ripple @ base speed

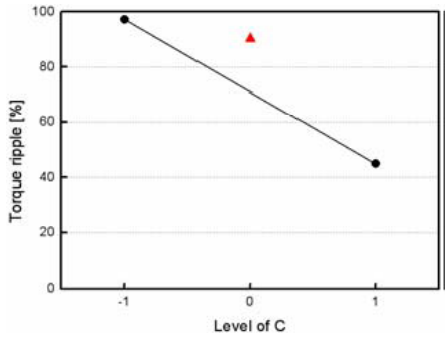

(b) Torque ripple @ maximum speed

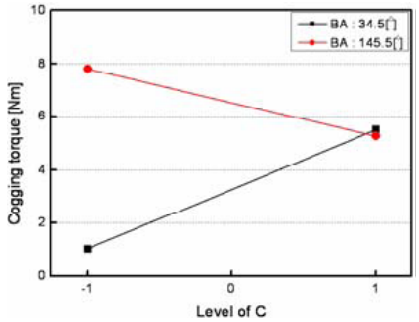

(c) Cogging torque

Fig. 6 Responses according to the variation of main factors

Central composite design (CCD) is employed as the experimental design method to estimate the fitted model of each response [9]. CCD consists of three portions: a complete 2^k factorial design in which the factor levels are coded into –1 and 1; axial points at a distance α from the center point; one design center point. Table VII shows the design area of CCD based on FFD results. At that time, the width of SO is restricted to 9 mm to support coil in the slot.

From the above stated process, the polynomial models of the responses are given by (15), (16) and (17) respectively

$$Y_{Tr\_base} = 48.4 + 0.16 \times BA - 17.9 \times C - 6.4 \times SO - 0.002 \times BA^2 + 4.1 \times C^2 + 0.1 \times SO^2 - 0.04 \times BA.C + 0.008 \times BA.SO + 1.7 \times C.SO \qquad (15)$$

TABLE III
DESIGN REGION OF CCD

Design factors	Levels of design factors	Levels of design factors	Levels of design factors	Levels of design factors	Levels of design factors
	-α	-1	0	1	α
BA [°]	25.25	29	34.5	40	43.75
C [mm]	0.16	0.5	1.0	1.5	1.84
SO [mm]	5.32	6	7	8	8.68

TABLE VI
OPTIMAL POINTS OF EACH RESPONSE

Design Factors torque	Optimal point @ base speed	Optimal point @ max. speed	Optimal point @ cogging
BA [°]	25.25	25.25	43.75
C[mm]	0.53	1.84	0.5
SO[mm]	8.68	8.68	8.68

$$Y_{Tr\_max} = 145.8 + 2.1\times BA - 140.5\times C + 7.4\times SO - 0.03\times BA^2 + 5.7\times C^2 - 2.6\times SO^2 - 0.3\times BAC + 0.1\times BASO + 12.2\times CSO \quad (16)$$

$$Y_{CT^{\wedge}} = 11.7 + 0.3\times BA - 3.8\times C + 2.4\times SO + 0.003\times BA^2 + 2.5\times C^2 - 0.1\times SO^2 + 0.02\times BAC - 0.03\times BA.SO + 0.3\times C.SO \quad (17)$$

Table III displays the optimal points minimizing each response obtained by (14), (15) and (16), and Fig. 7 shows the results of each model corresponding to the point. As known in the results, the optimal conditions can not simultaneously minimize torque ripple at the base and maximum speed andcogging torque. Moreover, each optimal point with respect to torque ripple at the maximum speed and cogging torque is located contrastively. That means the appropriate trade-off is required according to the application of IPMSM. As SO is 8.68 mm, the variation of each response is shown in Fig. 8.

In each optimal point, the results from the polynomial models are compared with those of FEA in Table IX. From the comparison, the models are very useful to predict the responses in the region. That is also verified by the coefficient of determination called R^2 [9], [10]. It is the statistics index to evaluate the quality of the models. R^2 of each fitted model are 0.985, 0.996 and 0.927 respectively.

V. CHARACTERISTIC ANALYSIS OF LOSSES

When the optimization is performed in Section IV, the losses is not considered. Thus, if the losses is considered, the results of Table IX is not guaranteed because input current and

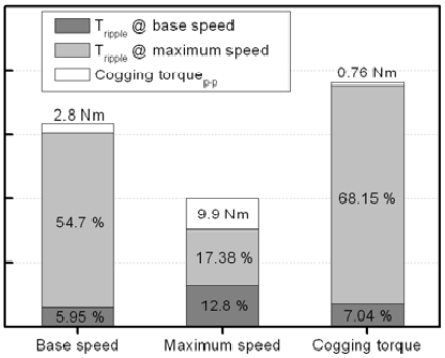

Fig. 7 Characteristics in optimal model of each response

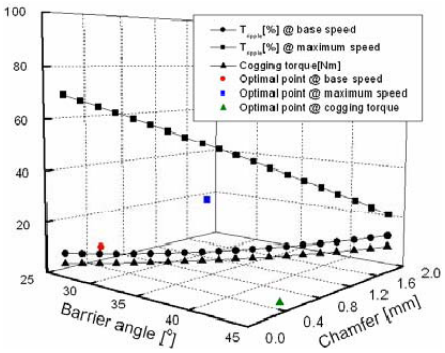

Fig. 8 Variation of each response according to design factors (SO: 8.68 mm)

β may be vary. In this Section, the characteristics of initial and optimal models are examined and analyzed when all the losses are considered.

A. Characteristic Prediction

The losses must be estimated to get the characteristic of each model. In this paper, R_c is calculated with the method proposed in Section III, and mechanical loss of all the models is the same and proportional to the square of mechanical speed [4]. At that time, the mechanical loss at 1000 rpm is standard, and it is defined as 0.5% of rated output power. Table X shows final results of each model considering the losses. The characteristic of the optimal model at the maximum speed is somewhat different as compared with other models. That is generated because of decrease of flux linkage by the chamfer. Therefore, as the optimization is performed at the maximum speed, the restrictions are required to satisfy the characteristics given in the specifications.

B. Torque Characteristic of Each Model

The torque waveform at the base and maximum speed and cogging torque of each model are shown in Fig. 9 and Fig. 10. At the base speed, the conditions, input current and β, of initial model are not greatly changed as compared with the original that because the influence of mechanical and iron loss is small. However, β of the optimized models considerably varies due to the decrease of back-EMF. So, torque ripple displayed in Fig. 9 differs from those given in Table IX.

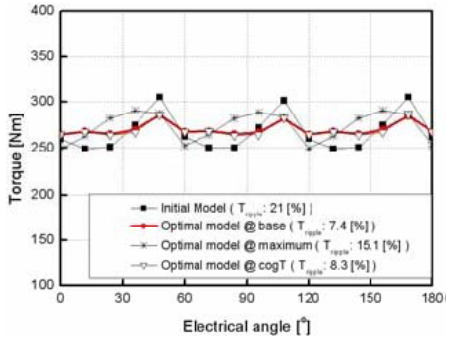

(a)@ Base speed

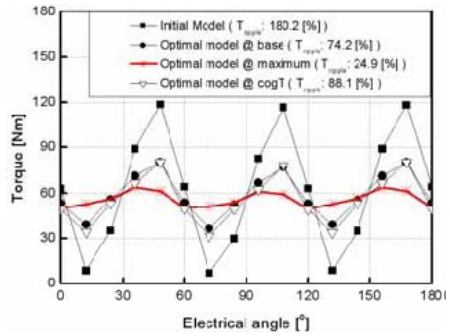

(b) @ Maximum speed

Fig. 9 Torque comparison of each model

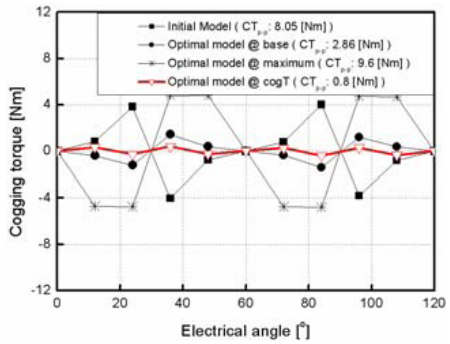

Fig. 10 Cogging torque comparison of each model

VI. Conclusion

In this paper, an optimization method was proposed to improve torque performance of the IPMSM with concentrated winding and wide speed range, and the results by the method showed the optimization shape in each speed region is different. Moreover, as the optimal design is performed at the maximum speed, the particular care is required. Finally, the optimization direction of the IPMSM with concentrated winding operated in the wide speed range must be changed according to the application of the IPSMS.

Acknowledgment

The authors are grateful to A. Fadaie, E. Baradar and V. Darvish from Sharif University, for their thorough observations. They also wish to thank Prof. M. Isapour and A. R. Gholipour from Lasckosch Research group and Prof. H. Lesani from University of Tehran for their insightful ideas and comments.

References

[1] John M. Miller, *Propulsion systems for hybrid vehicles*, The Institution of Electrical Engineers, 2004.
[2] Mohammad S. Islam, S. Mir, T. Sebastian, and S. Underwood, "Design consideration of sinusoidally excited permanent magnet machines for low torque ripple applications," *in Conf. Rec. IEEE-IAS Annu. Meetings*, 2004, CD-ROM.
[3] M. Sanada, K. Hiramoto, S. Morimoto, and Y. Takeda, "Torque ripple improvement for synchronous reluctance motor using an asymmetric flux barrier arrangement," *IEEE Trans. Ind. Applicat.*, vol. 40, no. 4, pp. 1076-1082, July/August 2004.
[4] S. Morimoto, Y. Tong, Y. Takeda, and T. Hirasa, "Loss minimization control of permanent magnet synchronous motor drives," *IEEE Trans. Ind. Electron.*, vol. 41, no. 5, pp. 511-517, Oct. 1994.
[5] J. J. Lee, Y. K. Kim, H. Nam, K. H. Ha, J. P. Hong, and D. H. Hwang, "Loss distribution of three phase induction motor fed by pulsewidth-modulated inverter," *IEEE Trans. Magn.*, vol. 40, no. 2, pp. 762-765, Mar. 2004.
[6] S. Morimoto, Y. Takeda, and T. Hirasa, "Current phase control methods for permanent magnet synchronous motors," *IEEE Trans. Power Electron.*, vol. 5, no. 2, pp. 133-138, April 1990.
[7] S. Morimoto, and Y. Takeda, "Machine parameters and performance of interior permanent magnet synchronous motors with different permanent magnet volume," *Elec. Eng. in Japan*, vol. 131, no. 4, pp. 1403-1408, 2000.
[8] Douglas C. Montgomery, *Design and Analysis of Experiments*, John Wiley & Sons, 2001.
[9] Raymond H. Myers and Douglas C. Montgomery, *Response Surface Methodology: Process and Product Optimization Using Design Experiments*, John Wiley & Sons, 1995.
[10] J. T. Li, Z. J. Liu, M. A. Jabbar, and X. K. Gao, "Design optimization for cogging torque minimization using response surface methodology," *IEEE Trans. Magn.*, vol. 40, no. 2, pp. 1176-1179, March 2004.

Mehdi K. Zadeh was born in Dezfoul, Iran, on January 2, 1983. He received the B.Sc. degree from the Electrical Engineering Faculty of the University of Tehran Sh., Tehran, Iran, in 2007, in Communication Engineering.

He is presently a graduate student working towards his Master's degree at the University of Tehran, in Power Electronics Engineering. He is member of power systems and machines research lab in Department of Electrical Engineering in University of Tehran.

His research interests are related to control of Electrical Drives, Power Electronics, FACTS, and Finite Element Method for Analysis of Electrical Machines and HVDC.

Ehsan M. Siavashi was born in Sari, Iran, on April 5, 1984. He received the B.Sc. degree from the Electrical Engineering Faculty of the Khajeh Nasir Toosi University of Technology (KNTU), Tehran, Iran, in 2007, in Electronic Engineering. In 2007, he joined the Electrical Engineering Faculty of the University of Tehran, where he is presently a graduate student working towards his Master's degree at the University of Tehran, in Power Electronics Engineering.

He is member of power systems research lab in Department of Electrical Engineering in University of Tehran.

His main scientific interests are related to Power Electronics, Control of Electrical Drives, FACTS, Parameter and State Estimation and Adaptive Algorithms.